PHOTOSYNTHETICA
International Journal for Photosynthesis Research

DOI 10.32615/ps.2023.035 PHOTOSYNTHETICA 61 (SI): 441-450, 2023

Special issue in honor of Prof. Győző Garab

The impact of physiologically relevant temperatures on physical properties of thylakoid membranes: a molecular dynamics study

B. FEHÉR[*,+], I.K. VOETS[*], and G. NAGY[**,+]

Laboratory of Self-Organizing Soft Matter, Department of Chemical Engineering and Chemistry, Eindhoven University of Technology, P.O. Box 513, 5600 MB Eindhoven, The Netherlands[*]
Neutron Scattering Division, Oak Ridge National Laboratory, Oak Ridge, Tennessee 37831, USA[**]

Abstract

Thylakoid membranes are energy-converting membranes with a unique lipid composition. Though the membranes are primarily composed of proteins, their photosynthetic function is strongly influenced by the lipid constituents. Here we characterize, with molecular dynamics (MD) simulations, lipid bilayers with compositions representative of plant thylakoid membranes. We determine, in a wide range of temperatures, the physical parameters of the model membranes which are relevant for the photosynthetic function. We found a marked impact of temperature on membrane permeability due to a combination of increased compressibility and curvature of the membrane at elevated temperatures. With increasing temperatures, we observed increasingly smeared transmembrane density profiles of the membrane forming lipid headgroups predicting increased membrane flexibility. The diffusion coefficient of the lipids increased with temperature without apparent specificity for lipid species. Instead of a comprehensive experimental dataset in the relevant temperature range, we quantitatively compared and validated our MD results with MD simulations on a dipalmitoylphosphatidylcholine model system.

Keywords: mechanical properties; molecular dynamics; permeability; thylakoid.

Introduction

Photosynthetic thylakoid membranes are the most abundant membranes on earth and are fundamental to the energy cycle of the biosphere. Not only do they host the proteins participating in the light reactions of photosynthesis, but they also serve as a physical barrier, allowing for the build-up of an electrochemical gradient across

Highlights

- Nanoscale clustering is observed in thylakoid lipid membrane models
- The model membrane is highly flexible
- Compressibility modulus and curvature influence temperature-dependent permeability

Received 10 July 2023
Accepted 11 September 2023
Published online 10 October 2023

[+]Corresponding authors
e-mail: b.feher@tue.nl (B. Fehér)
nagyg@ornl.gov (G. Nagy)

Abbreviations: CG – coarse graining; DFGG – DGDG with di-18:3 acyl chains; DFMG – MGDG with di-18:3 acyl chains; DGDG – digalactosyldiacylglycerol; DPPC – dipalmitoylphosphatidylcholine; FPGG – DGDG with 18:3/16:0 acyl chains; FPMG – MGDG with 18:3/16:0 acyl chains; FPSG – SQDG with 18:3/16:0 acyl chains; JFPG – PG with 16:1(3t)/18:3 acyl chains; JPPG – PG with 16:1(3t)/16:0 acyl chains; LHCII – main light-harvesting protein complex of PSII; MD – molecular dynamics; MGDG – monogalactosyldiacylglycerol; MSD – mean-squared displacement; PG – phosphatidylglycerol; *Scd* – so-called deuterium order parameter; SQDG – sulfoquinovosyldiacylglycerol; TLM – thylakoid lipid membranes.

Acknowledgments: We wish to thank Dr. Győző Garab for the discussions related to the role of lipids in the photosynthetic membrane functions and for the inspiration and support throughout our scientific career. The authors acknowledge [KIFÜ] for awarding us access to resources based in Hungary at Debrecen for CPU time. A portion of this research used resources at the Spallation Neutron Source, a DOE Office of Science User Facility operated by the Oak Ridge National Laboratory.

Conflict of interest: The authors declare that they have no conflict of interest.

the inner (luminal) and outer aqueous phases of the thylakoid membrane. Thylakoid membranes are rich in proteins, which occupy about 70% of the total area of thylakoid membranes. The remaining 30% is covered by lipid molecules (Kirchhoff *et al.* 2002). Whilst the photosynthetic machinery responsible for light harvesting and conversion is mostly composed of thylakoid proteins, the role of the lipids extends beyond providing a scaffold. The importance of lipid–protein interactions for the functioning of membrane proteins is increasingly recognized (Jodaitis *et al.* 2021). The key lipids in plant thylakoid membranes are (in decreasing order of abundance): the neutral galactolipids monogalactosyldiacylglycerol (MGDG) and digalactosyldiacylglycerol (DGDG), the charged glycolipid sulfoquinovosyldiacylglycerol (SQDG), and the charged phospholipid phosphatidylglycerol (PG). It is important to note the high fraction of MGDG, which does not form bilayers on its own. MGDG are also abundant and critical for the functioning of other energy-converting membranes (*cf.* phosphatidylethanolamine and cardiolipin in mitochondria) (Basu Ball *et al.* 2018, Garab *et al.* 2022). Small changes in the lipid composition of thylakoid membranes may have large impacts on the development, structure, and functionality of the membrane system (Kobayashi 2016). Understanding the structural and functional characteristics of the constituent lipids of thylakoid membranes is indispensable for an in-depth comprehension of the operation of protein-rich thylakoids.

Molecular dynamics (MD) simulations have been widely applied to achieve a molecular-level understanding of lipid membranes (Hollingsworth and Dror 2018, Róg *et al.* 2021, Watkins 2023), ranging from one-component systems to complex, multi-component membranes with and without membrane proteins (Chavent *et al.* 2016). In all-atom explicit solvent molecular dynamics (MD) simulations, Newton's equations are solved for all atoms in the system to calculate the trajectories of all atoms over time (Abraham *et al.* 2015). For large systems, such as biological membranes, coarse-graining (CG) is essential to complete a computation within a reasonable simulation time (de Jong *et al.* 2013). In a CG simulation, four atoms are represented by a bead, and the potentials are determined between these beads. As a result, the number of elementary particles decreases significantly, which allows us to perform longer simulations (in the microsecond range) to cover the whole conformational space.

MD simulations have shed light on different substructures of the photosynthetic system in the past; van Eerden *et al*. (2015) investigated the properties of thylakoid membranes of cyanobacteria and higher plants. They found that the lateral separation of lipids does not occur at the molecular level and that cyanobacterial thylakoid membranes are less fluid than those of higher plants. Furthermore, van Eerden *et al*. (2015) demonstrated that plant membranes tend to form inverted hexagonal phases. Other works focused on the properties of the PSII complex within the membrane and the mechanism of cofactor binding (van Eerden *et al.* 2017a,b,c). Their work presents that PSII requires several tens of μs of time to equilibrate, which is important to keep in mind for the sake of ergodicity. They found that in the vicinity of PSII, MGDG and SQDG lipids accumulate due to electrostatic interactions. Another study investigated the main light-harvesting protein complex of PSII (LHCII) in the membrane and concluded that, like PSII, MGDG enrichment occurs in the surroundings of LHCII (Thallmair *et al.* 2019). This MGDG enrichment was attributed to the steric compatibility of the protein and lipid molecule. Interestingly in another article focusing on the behavior of LHCII in thylakoid membranes – with or without an associated PSII subunit – accumulation of the DGDG was observed by Daskalakis and collaborators at the luminal side of the LHCII trimer at low pH (Daskalakis *et al.* 2019). In recent atomistic simulations performed on thylakoid lipids of a red alga, Rathod and collaborators found a temperature-dependent phase behavior. Key structural properties, such as the magnitude of the lipid chain order parameter, the presence and size of nanodomains, and membrane thickness, are affected by temperature variations from 283 to 313 K (Rathod *et al.* 2023).

Herein we present coarse-grained molecular dynamics simulations to determine the effect of temperature on various properties of plant thylakoid lipid membranes (TLM) from 270 to 330 K – a range chosen for physiological relevance and for the applicability of the employed simulation tools (Bruininks *et al.* 2019). We investigated features such as membrane thickness and self-diffusion of the lipid components of the membrane and compared these to the temperature dependence of the properties of a dipalmitoylphosphatidylcholine (DPPC) reference membrane, whose properties are well-established. Furthermore, we analyzed the mechanical behavior of the membranes such as rigidity, curvature, and permeability. In addition to the importance of understanding the response of TLMs to temperature, the presented results will serve as a well-characterized starting point for simulations targeting further physiologically relevant questions.

Materials and methods

Coarse-grained molecular dynamics simulation was performed with *Gromacs 2019.6* (Pronk *et al.* 2013, Abraham *et al.* 2015). The initial configuration of bilayers was constructed by the *CHARMM-GUI* server (Jo *et al.* 2007, 2008, 2009; Brooks *et al.* 2009, Wu *et al.* 2014, Lee *et al.* 2016, 2019). The system was composed of 1,400 lipids, 16:1(3t)-16:0 and 16:1(3t)18:3 PG, 18:3(9,12,15)-16:0 and di18:3(9,12,15) DGDG, 18:3(9,12,15)-16:0 and di18:3(9,12,15) MGDG and 18:3/16:0 SQDG lipids. On both sides of the membrane, a 2.25-nm water layer was placed. For better understanding, we tabulated the different lipids and corresponding notations in the table below alongside the composition of the two leaflets, which is symmetrical.

Coarse-grained simulations were performed using a Martini 2.2p force field (de Jong *et al.* 2013) with a polarizable water model (Yesylevskyy *et al.* 2010) with relative permittivity of the medium set to 2.5. Na^+ and Cl^- ions were used to charge neutralize the system. The structures were minimized for 5,000 steps using

Lipid family	Acyl chains	Used notation in the present paper	Number [per leaflet]
PG	16:1(3t)/18:3	JFPG	70
	16:1(3t)/16:0	JPPG	35
MGDG	di-18:3	DFMG	245
	18:3/16:0	FPMG	35
DGDG	di-18:3	DFGG	175
	18:3/16:0	FPGG	35
SQDG	18:3/16:0	FPSG	105

the steepest descent method, followed by 3,000 ps equilibration in three steps with integration time step from 2 fs to 10 fs. The reaction field method was applied to calculate the long-range electrostatic interactions (Tironi *et al.* 1995) with a 1.1-nm cutoff distance. Van der Waals interactions were treated with a cutoff of 1.1 nm. The temperature was kept constant with the velocity rescaling thermostat (Bussi *et al.* 2007) with 1 ps coupling time at 270, 280, 290, 300, 310, 320, and 330 K. The pressure was semi-isotropically coupled and maintained by Berendsen barostat with 12 ps coupling time (Berendsen *et al.* 1984). The production run was performed for 1,000 ns with Parrinello-Rahman barostat with 12 ps coupling time (Parrinello and Rahman 1981). Three independent simulations were performed on each temperature and the obtained values averaged over the three runs. The input for the simulation of stacked bilayers was constructed by copying the final snapshot of the production run of mono-bilayer systems in the z direction and the simulation scheme was identical to the described protocol. As a control, a membrane consisting of 1,400 DPPC molecules was simulated with the same protocol. Visualization and manipulation of coordinate files were performed by *PyMOL* (The *PyMOL Molecular Graphics System*, *version 2.0*, *Schrödinger*, LLC). Membrane thickness was calculated by *Membrane Plugin*, *version 1.1* (Guixà-González *et al.* 2014) implemented in *Visual Molecular Dynamics* (VMD) (Humphrey *et al.* 1996). The mean average curvature was calculated with a slightly modified version of the *MDAnalysis MembraneCurvature Python* toolkit (Michaud-Agrawal *et al.* 2011, Gowers *et al.* 2016) to extract the maximum curvature of each frame.

Results and discussion

Visual inspection and lipid clustering: Top and side views of snapshots of the simulation at 300 K are presented in Fig. 1. The side view snapshot at 1,000 ns suggests a dynamic membrane with continuous fluctuation. The top view images at 0 and 1,000 ns reveal a slight degree of clustering of DFMG and DFGG lipids.

For a more quantitative grip on clustering events, the so-called contact matrix was calculated. All beads of each molecule were taken into account and the number of contacts with beads of other molecules was calculated at the beginning and averaged over the second five hundred nanoseconds of the simulation based on the proximity of the beads. Two beads are considered to be in contact when their distance from each other is less than 0.5 nm. The number of contacts at the end of the simulation was normalized to the number of contacts at the initial configuration. Consequently, if the normalized contact number is greater than 1, they tend to cluster together and when it is less than 1, they tend to migrate away from each other. Interestingly, the contact matrix (Fig. 2) also suggests that different pairs of lipids tend to cluster. Clustering is pronounced for both JPPG and FPMG, which tend to be surrounded by lipids of the same type rather than other types of lipids. The matrix suggests significant clustering for FPGG with FPMG and the modest clustering of JFPG, DFMG, and FPGG (10% increase in number of contacts),

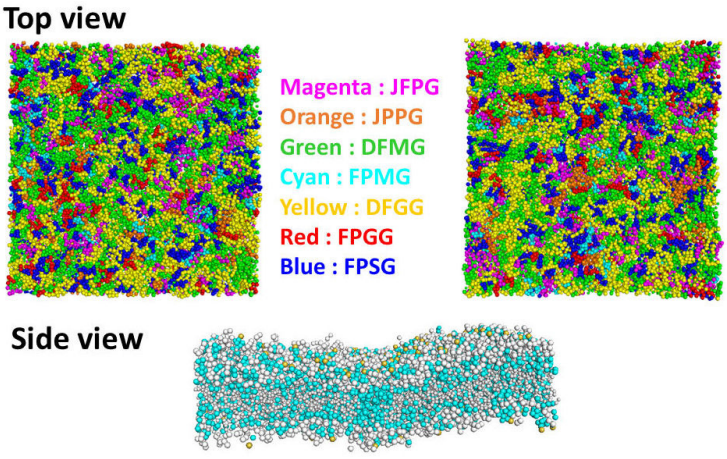

Fig. 1. Representative snapshots from the simulation at 300 K. DFGG – DGDG with di-18:3 acyl chains; DFMG – MGDG with di-18:3 acyl chains; FPGG – DGDG with 18:3/16:0 acyl chains; FPMG – MGDG with 18:3/16:0 acyl chains; FPSG – SQDG with 18:3/16:0 acyl chains; JFPG – PG with 16:1(3t)/18:3 acyl chains; JPPG – PG with 16:1(3t)/16:0 acyl chains.

which may or may not be significant. Furthermore, JPPG with JFPG, FGPP with JFPG, FPSG with JFPG, FPMG with JPPG, and FPGG with FPMG accumulate in proximity of each other. These results suggest that the distribution of lipids is not random within the membrane. In other words, the lipids have a preferred local environment which differs in lipid composition from the overall mean composition. One could speculate that the van der Waals interactions and the electrostatic repulsive and attractive forces overlap with the contact matrix, which is partially true. However, it is interesting to note that the most significant clustering occurs between the negatively charged JPPGs, which suggests that the van der Waals forces overcome the electrostatic repulsion in the complex environment.

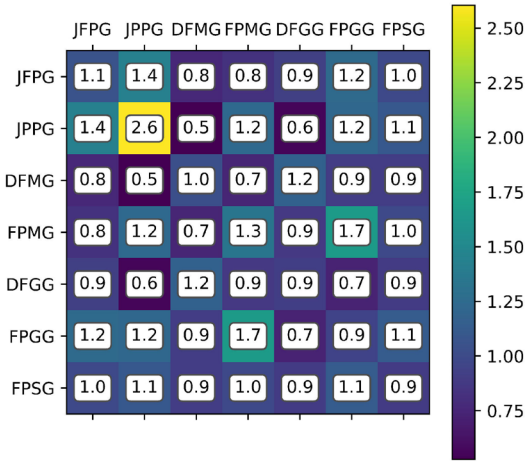

Fig. 2. Time-averaged contact matrix of lipid species at the second half of the simulation normalized to the initial configuration. DFGG – DGDG with di-18:3 acyl chains; DFMG – MGDG with di-18:3 acyl chains; FPGG – DGDG with 18:3/16:0 acyl chains; FPMG – MGDG with 18:3/16:0 acyl chains; FPSG – SQDG with 18:3/16:0 acyl chains; JFPG – PG with 16:1(3t)/18:3 acyl chains; JPPG – PG with 16:1(3t)/16:0 acyl chains.

Density profiles of lipid and water: First, the cross-section density profile of the bilayers along the bilayer normal was calculated. The analysis was performed on the second half of the simulation (after 500 ns) to investigate the equilibrated system. The head groups were defined as phosphate bead (PO4) for JPPG and JFPG, C1 (a member of the galactosyl group) for DFMG, FPMG, and FPSG; and finally, GA2 (a member of the galactosyl group further from the acyl chain) for FPGG and DFGG. The profiles of the headgroups and the profile of water density along the bilayer normal are presented in Fig. 3*A* and Fig. 3*B*, respectively, for different temperatures. The density profiles of the headgroup exhibit the usual profile for headgroups at low temperatures. They show two well-defined peaks and in the middle of the bilayer, they reach a minimum close to 0. This suggests a well-defined bilayer with small fluctuations of the molecules. However, with increasing temperature, the density at the maxima gradually decreases whilst at the minima increases. This phenomenon is well expressed above 300 K, indicating that at higher temperatures the fluctuation of the molecules is more favorable which smears the density profile. This also predicts a higher flexibility of the membrane at higher temperatures. As it has been shown in Fig. 3*B*, at low temperatures, the water molecules cannot penetrate the center of the bilayer while at higher temperatures (above 300 K), a slight penetration of water is observed.

In Fig. 4, we display the histogram of thicknesses of the membrane at different temperatures. As a reference, we also show the thickness of a DPPC membrane. For DPPC, the thickness is around 4.2 nm while for TLMs around 3.7 nm. These results suggest that the thylakoid membrane at any temperature is more fluid than the DPPC and its resistance against buckling (fluctuation of the membrane

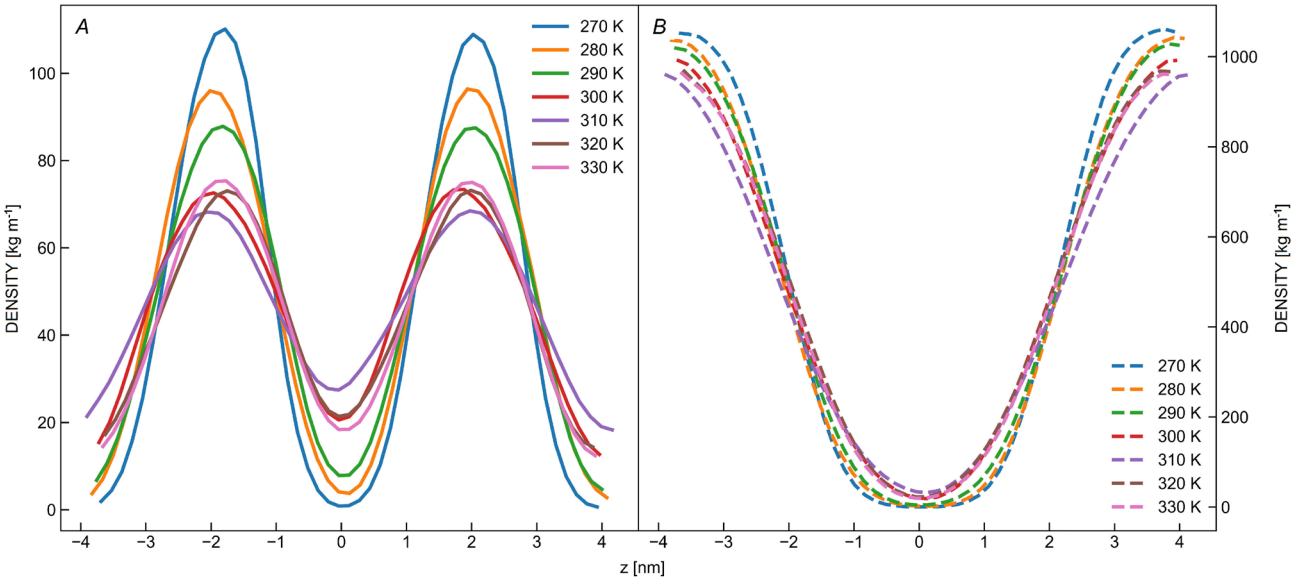

Fig. 3. Profiles of the headgroups (*A*) and the profile of water density (*B*) along the bilayer normal of the thylakoid lipid membranes.

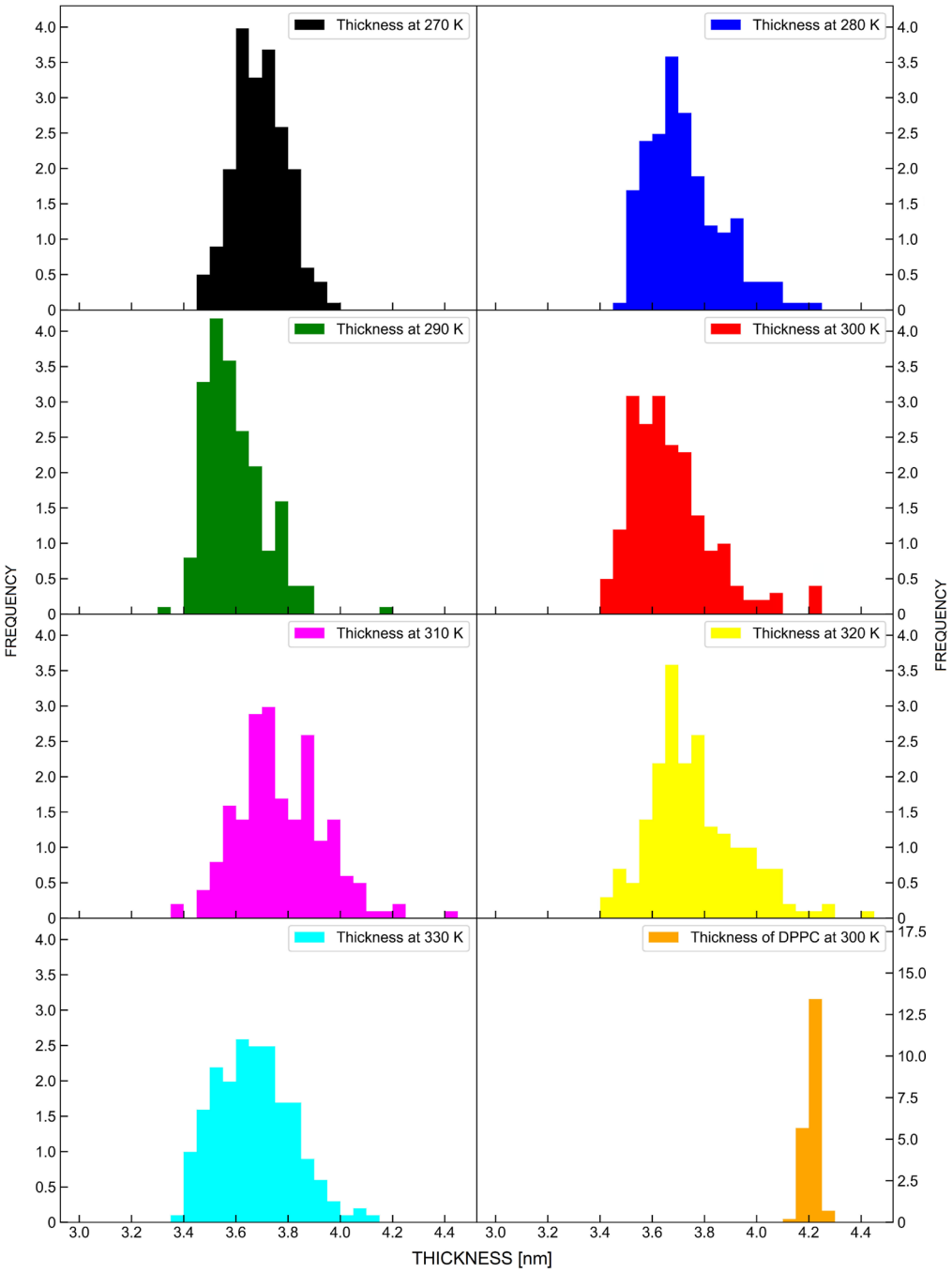

Fig. 4. Histograms of the thickness of DPPC at 300 K and thylakoid membranes at different temperatures over time.

in the direction of bilayer normal) is lesser which allows it to fluctuate more. However, clear temperature dependence cannot be observed.

Order parameter: To further elaborate the phase behavior of the membrane, we calculated the so-called deuterium order parameter (*Scd*) (Tieleman *et al.* 1997, Song *et al.* 2005, Chen *et al.* 2014, Piggot *et al.* 2017). *Scd* was calculated individually for all lipids' sn-1 and sn-2 chains. The *Scd* is averaged over the lipid tails and time and represents the ordering of lipid tails along the bilayer normal. *Scd* is defined as

$$Scd = \frac{\left\langle 3\cos^2\theta - 1 \right\rangle}{2} \quad (1)$$

where θ is the angle between the C–H bond vector and the bilayer normal. The angle brackets stand for molecular and temporal ensemble averages (Piggot *et al.* 2017).

The *Scd* was calculated and averaged for the last 500 ns of the simulation. The *Scd* graphs are presented in

Fig. 1S (*supplement*). In all cases, we observed a gradual decrease of the *Scd* which suggests gradual disordering of the lipid tails instead of a sharp 'melting temperature'. Note that since the *Scd* values are small even at the most ordered state we are likely facing fluid membranes even at low temperature. Interestingly, in the case of JFPG (C16:1(3t)/18:3 PG), FPGG (18:3/16:0), FPMG (18:3/16:0), and FPSG (C18:3/16:0) the sn-1 and sn-2 chains display quite different behavior. This is somewhat expected since these lipids are asymmetric in terms of the hydrocarbon chain, in most cases (except JFPG) with a tail with a mono-unsaturated 18-carbon chain and a saturated 16-carbon chain. In the case of JFPG, the chain with 16 carbon atoms is also mono-unsaturated. In the case of JFPG, the sn-2 chain (linolenoyl tail 18 carbons) is aligned more along the bilayer normal than the sn-1 chain, while in other cases the other way round. In the case of FPGG, FPMG, and FPSG, the saturated sn-2 chain shows less ordering. In the case of JPPG (16:1(3t)/16:0), DFGG (di-C18:3 DGDG), and DFMG (di-C18:3 MGDG), sn-1 and sn-2 chains show quite similar behavior, which can be attributed to the same or only slightly different carbon chains.

Increased mobility at elevated temperatures: To study the effect of temperature on the mobility of thylakoid membrane lipids, we calculated the translational diffusion coefficients of each lipid for each temperature (Fig. 5). The diffusion coefficient was determined by fitting a straight line to the mean-squared displacement of lipids as a function of time (Eq. 1).

$$MSD = 2Dt \tag{2}$$

where *MSD* is the mean-squared displacement, *D* is the diffusion coefficient and *t* is time.

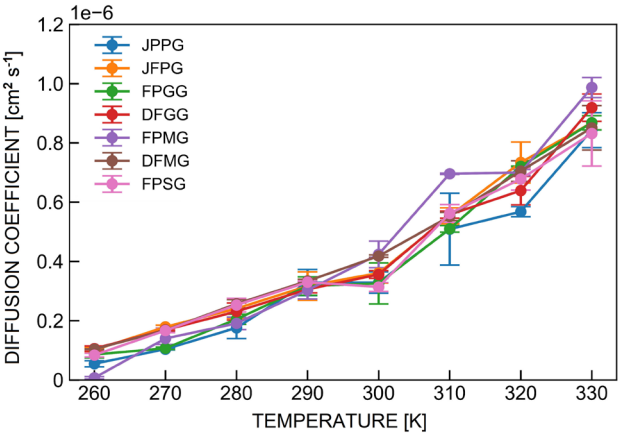

Fig. 5. Diffusion coefficient of the different lipid species as a function of temperature. DFGG – DGDG with di-18:3 acyl chains; DFMG – MGDG with di-18:3 acyl chains; FPGG – DGDG with 18:3/16:0 acyl chains; FPMG – MGDG with 18:3/16:0 acyl chains; FPSG – SQDG with 18:3/16:0 acyl chains; JFPG – PG with 16:1(3t)/18:3 acyl chains; JPPG – PG with 16:1(3t)/16:0 acyl chains.

As expected, all lipid species become more mobile at elevated temperatures. We attribute this to an increase in thermal energy (which increases lipid mobility) and to an increase in membrane fluidity. It is important to emphasize that we focus here on the informative trends rather than the absolute values of the diffusion coefficients, which are not representative of experimental values due to the lack of atomistic details (CG simulations underestimate the diffusion coefficient) (van Eerden *et al.* 2017c). The presented results at 290 K, however, are in good agreement with the CG results presented for plant membranes with CG simulation at 293 K (van Eerden *et al.* 2015). The authors are not aware of lipid diffusion measurements on systems with compositions representative of that of thylakoids, diffusion constants in phospholipid bilayers are documented to have similar magnitude (Gaede and Gawrisch 2003, Gupta *et al.* 2019).

Large compressibility modulus: The compressibility modulus describes the resistance of the bilayer against compression. The smaller the compressibility modulus is, the more compressible the membrane. The compressibility modulus is related to the fluctuation of lipid area per molecule and can be expressed as

$$K_A = \frac{kTA_0}{N\left\langle \delta A_0^2 \right\rangle} \tag{3}$$

where K_A is the compressibility modulus, A_0 is the average area per molecule during the simulation, N is the number of molecules and $\left\langle \delta A_0^2 \right\rangle$ is the fluctuation of area per molecule. For a detailed description refer to Feller *et al.* (*e.g.*, Feller and Pastor 1999). The compressibility modulus as a function of temperature is tabulated in Table 1. As can be seen, the value decreases gradually up to 300 K while above that temperature it seems to fluctuate around a constant value. This is in line with our observation regarding the density profiles where we saw gradual smearing of the peaks until 300 K, while above it the change of the profile is less pronounced. Interestingly, the compressibility modulus of DPPC at 300 K is 6 times larger than that of the TLM.

Permeability increases at elevated temperatures: The formation of the electrochemical gradient across the inner and outer aqueous phase of the thylakoid membrane is vital to its function, rendering the permeability of the membrane to protons, different solutes, and water to have crucial importance. The water permeability of the membrane at different temperatures was calculated as described by Venable *et al.* (2019). For the calculation, the simulation of a bilayer stack is required. To start the simulation, the last configuration of the production run at different temperatures was taken and copied in the z-direction, thus its initial volume is twice the volume of the equilibrated single bilayer. Equilibration and production runs were performed with the same parameters as for single bilayers. Subsequently, the number of water molecules diffused from between the two bilayers to outside and *vice versa* was counted as a function of time. If the total thickness

Table 1. Compressibility modulus of the lipid bilayer at different temperatures. Errors represent the standard deviation of the data obtained from averaging three independent runs.

Temperature [K]	Compressibility modulus/k_bT
270	22.40 ± 4.61
280	17.80 ± 3.11
290	11.03 ± 3.12
300	11.30 ± 0.29
310	9.72 ± 1.76
320	10.95 ± 0.71
330	9.16 ± 1.10
DPPC 300	62.46 ± 1.45

of water compartments is known (L), the permeability can be calculated by linear regression to the initial regime of crossing event – time function based in Eq. 3:

$$n_2(t) = \left(\frac{2NP}{L}\right)t \tag{4}$$

where $n_2(t)$ is the number of crossing events in the function of time, N is the number of water molecules, P is the permeability, and t is the time. The fitting procedure was performed in the first 20 ns. The reason for the short time taken into account for the regression is that Eq. 3 is the short time expansion of Fick's law, which describes the permeability on the time scale when re-crossing does not happen. Due to the high permeability of the membrane, this timescale is limited and found to be applicable at the first 20 ns in our system based on the initial linear range of the curves. The crossing event–time function is plotted in Fig. 6 and the results of the linear regression are presented in Table 2. A drastic increase in the number of crossing events can be observed in Fig. 6. Between 270 and 290 K the number of crossings does not change significantly; on the other hand, increasing the temperature to 300 K, a threefold increase is observable. This drastic step coincides with the pronounced decrease in the compressibility modulus of the membrane, which suggests that the increased fluidity of the membrane has a dramatic effect on the permeability. Increasing the temperature from 310 to 330 K, a gradual and significant increase is displayed. The quantitative results support the visual observation from the curves. Comparing the values with the permeability values calculated for dilauroylphosphatidylcholine (DLPC) in the work of Venable *et al.* (2019), our result at 300 K is two orders of magnitude greater ($4.2 \times 10^{-12} \pm 1.2 \times 10^{-12}$ cm ns^{-1} in cited paper). To further demonstrate the high permeability of thylakoid membrane compared to phosphatidylcholine, we simulated and performed the same analysis on DPPC at 300 K. The obtained permeability is $5.6913 \times 10^{-12} \pm 1.0819 \times 10^{-14}$ cm ns^{-1}, which is in agreement with the literature cited above, thus further supports our observation. The connection between permeability and compressibility is also pronounced according to the high compressibility modulus and low permeability of DPPC.

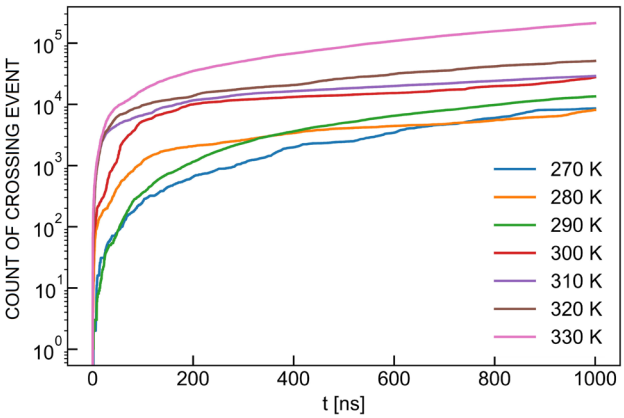

Fig. 6. Number of water crossing events across the lipid bilayer as a function of time and temperature.

Table 2. Permeability of membrane at different temperatures. Errors were obtained by linear regression.

Temperature [K]	Permeability [cm ns^{-1}]
270	$9.081 \times 10^{-11} \pm 1.562 \times 10^{-12}$
280	$5.510 \times 10^{-10} \pm 6.061 \times 10^{-12}$
290	$5.513 \times 10^{-10} \pm 6.064 \times 10^{-12}$
300	$9.307 \times 10^{-10} \pm 1.188 \times 10^{-11}$
310	$7.167 \times 10^{-09} \pm 2.522 \times 10^{-11}$
320	$6.867 \times 10^{-09} \pm 6.506 \times 10^{-11}$
330	$8.551 \times 10^{-09} \pm 6.755 \times 10^{-11}$
DPPC 300 K	$5.691 \times 10^{-12} \pm 1.082 \times 10^{-14}$

Different mechanisms of increased permeability below and above 310 K: Yesylevskyy *et al.* (2019) found from MD simulations that the permeability of mammalian plasma membrane for water and ions was enhanced by generating curvature. To decide whether the significantly enhanced permeability has a correlation with the curvature of the thylakoid membrane at elevated temperatures or if it can be entirely attributed to the increased chain dynamics, the mean curvature of the bilayers at each temperature was calculated by the *MDAnalysis* tool. Since the membrane is dynamically moving and the local curvatures are not maintained by additional components (*e.g.*, proteins) or external force, the averaged mean curvature through the whole trajectory would not be informative. Thus, the mean curvature of each configuration was determined, and the maximum values were collected into a histogram. This representation allows us to visually observe if at higher temperatures higher mean curvature is more probable. The results are presented in Fig. 7. As can be seen, the maximum of the histogram does not noticeably shift to higher values as a function of temperature. Above 310 K, the probability of maximum curvature above 5 Å^{-1} slightly increases. To get a more quantitative insight into the difference of the histograms, we calculated the first four central momenta from which the first and the second momentum is the mean and variance respectively, whilst

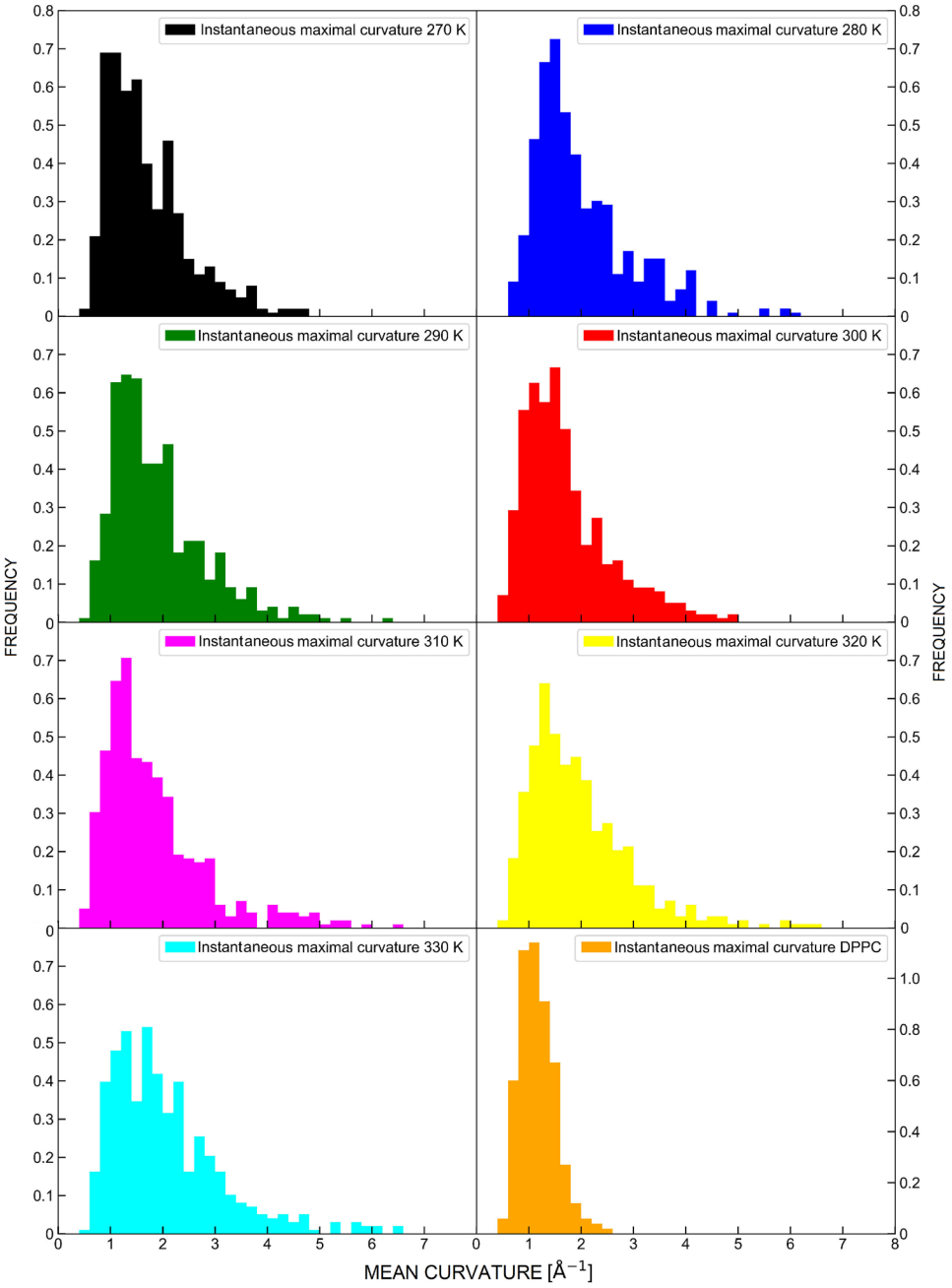

Fig. 7. Mean curvature of the lipid bilayer as observed at different temperatures.

the third and fourth standardized momentum is the skewness and kurtosis. The momenta are collected in Table 3. From the results it can be concluded that the mean and variance become slightly bigger at and above 320 K. We propose the explanation that below 300 K the compressibility modulus decreases and above 300 K it stays constant while the mean and variance of the curvature is practically constant below 310 K and increases above 310 K. The combination of these three trends suggests different reasons for the increased permeability below and above 310 K. Below 310 K, the permeability is increased as a consequence of the increased compressibility of the membrane, while at the same time above 310 K, the permeability is facilitated by the slightly enhanced curvature. If we compare the curvature with DPPC it is clear from the histogram that it has a smaller mean value and variance. Calculating the momenta supports the visual observation. The mean value of DPPC at 300 K is approximately 40% smaller than the thylakoid at 300 K which supports the observation of Yesylevskyy *et al.* (2019) that increased curvature affects water permeability.

Conclusion: Thylakoid membranes are characterized by a unique lipid composition of predominantly galactolipids. The thylakoid lipids not only provide a scaffold for the photosynthetic membrane proteins but also have a strong

Table 3. Momenta of the probability distribution of maximum curvature at different temperatures. Errors represent the standard deviation of the data obtained from averaging three independent runs.

Temperature [K]	mean [Å^{-1}]	variance [Å^{-2}]	skewness	kurtosis
270	1.619 ± 0.034	3.488 ± 0.797	0.5785 ± 0.0851	0.9600 ± 0.1470
280	1.785 ± 0.176	3.997 ± 0.646	0.6240 ± 0.0123	1.0570 ± 0.0592
290	1.784 ± 0.021	4.322 ± 0.404	0.6603 ± 0.1066	1.1620 ± 0.2629
300	1.707 ± 0.091	3.896 ± 0.329	0.6092 ± 0.0765	0.9768 ± 0.1243
310	1.805 ± 0.090	4.455 ± 0.495	0.6283 ± 0.0969	1.0619 ± 0.1484
320	1.910 ± 0.052	5.245 ± 0.550	0.6301 ± 0.0395	1.0700 ± 0.1298
330	1.939 ± 0.018	5.315 ± 0.587	0.6341 ± 0.1008	1.0861 ± 0.1717
DPPC 300 K	1.055 ± 0.020	0.657 ± 0.050	0.4253 ± 0.0848	0.8895 ± 0.1540

influence on their function, oligomerization, long-range order, and even on photoprotective processes (Wilhelm *et al.* 2020). Herein we studied the effect of temperature on the properties of thylakoid lipid membranes relevant to photosynthesis. To this end, we performed a coarse-grained molecular dynamics simulation of lipid bilayers with compositions representative of membranes in higher plants. We found that at each temperature within the range of physiologically relevant temperatures, thylakoid membranes are more fluid and water-permeable than typical phosphatidylcholine membranes. Our simulations suggest that the increased water permeability is related to an increased compressibility and/or an increased curvature. The authors acknowledge the limitation of the physiological relevance of the presented results. First: the lipid composition of plants is known to be influenced both by heat (Higashi and Saito 2019) and cold stress (Barrero-Sicilia *et al.* 2017) therefore the presented temperature-dependent membrane characterization would be relevant only under short-term temperature variance conditions. Thermal stress is known to influence also the sterol content and composition of different plant species (Du *et al.* 2022), while sterols can be used to artificially alter the fluidity of thylakoid membranes (Velitchkova *et al.* 2009), though it is unclear if under naturally occurring increased contents of sterols the thylakoid membrane structure could be significantly influenced. Carotenoids are also shown to alter the structure and fluidity of the thylakoid membranes (Dell'Aglio 2021). Most importantly the composition of the thylakoid membranes is not dominated by lipids but rather by proteins with multi-level and functionally dynamic organization, which is expected to pose complex challenges for molecular dynamics simulations. This article therefore serves as a basis for future studies where we will elaborate on computational methods of thylakoid membrane model systems with increasing levels of complexity.

References

Abraham M.J., Murtola T., Schulz R. *et al.*: GROMACS: High performance molecular simulations through multi-level parallelism from laptops to supercomputers. – SoftwareX **1-2**: 19-25, 2015.

Barrero-Sicilia C., Silvestre S., Haslam R.P., Michaelson L.V.: Lipid remodelling: Unravelling the response to cold stress in *Arabidopsis* and its extremophile relative *Eutrema salsugineum*. – Plant Sci. **263**: 194-200, 2017.

Basu Ball W., Neff J.K., Gohil V.M.: The role of nonbilayer phospholipids in mitochondrial structure and function. – FEBS Lett. **592**: 1273-1290, 2018.

Berendsen H.J.C., Postma J.P.M., van Gunsteren W.F. *et al.*: Molecular dynamics with coupling to an external bath. – J. Chem. Phys. **81**: 3684-3690, 1984.

Brooks B.R., Brooks III C.L., Mackerell Jr. A.D. *et al.*: CHARMM: The biomolecular simulation program. – J. Comput. Chem. **30**: 1545-1614, 2009.

Bruininks B.M.H., Souza P.C.T., Marrink S.J.: A Practical View of the Martini Force Field. – In: Bonomi M., Camilloni C. (ed.): Biomolecular Simulations: Methods and Protocols. Pp. 105-127. Humana Press, New York 2019.

Bussi G., Donadio D., Parrinello M.: Canonical sampling through velocity rescaling. – J. Chem. Phys. **126**: 014101, 2007.

Chavent M., Duncan A.L., Sansom M.S.P.: Molecular dynamics simulations of membrane proteins and their interactions: from nanoscale to mesoscale. – Curr. Opin. Struct. Biol. **40**: 8-16, 2016.

Chen Z., Mao Y., Yang J. *et al.*: Characterizing the binding of annexin V to a lipid bilayer using molecular dynamics simulations. – Proteins **82**: 312-322, 2014.

Daskalakis V., Papadatos S., Kleinekathöfer U.: Fine tuning of the photosystem II major antenna mobility within the thylakoid membrane of higher plants. – BBA-Biomembranes **1861**: 183059, 2019.

de Jong D.H., Singh G., Bennett W.F.D. *et al.*: Improved parameters for the Martini coarse-grained protein force field. – J. Chem. Theory Comput. **9**: 687-697, 2013.

Dell'Aglio E.: Carotenoid composition affects thylakoid morphology and membrane fluidity. – Plant Physiol. **185**: 21-22, 2021.

Du Y., Fu X., Chu Y. *et al.*: Biosynthesis and the roles of plant sterols in development and stress responses. – Int. J. Mol. Sci. **23**: 2332, 2022.

Feller S.E., Pastor R.W.: Constant surface tension simulations of lipid bilayers: The sensitivity of surface areas and compressibilities. – J. Chem. Phys. **111**: 1281-1287, 1999.

Gaede H.C., Gawrisch K.: Lateral diffusion rates of lipid, water, and a hydrophobic drug in a multilamellar liposome. – Biophys. J. **85**: 1734-1740, 2003.

Garab G., Yaguzhinsky L.S., Dlouhý O. *et al.*: Structural and functional roles of non-bilayer lipid phases of chloroplast thylakoid membranes and mitochondrial inner membranes. – Prog. Lipid Res. **86**: 101163, 2022.

Gowers R., Linke M., Barnoud J. *et al.*: MDAnalysis: A Python

package for the rapid analysis of molecular dynamics simulations. – In: Proceedings of the 15th Python in Science Conference, Austin, Texas (July 11–17, 2016). Pp. 98-105. SCIPY, Austin 2016.

Guixà-González R., Rodriguez-Espigares I., Ramírez-Anguita J.M. *et al.*: MEMBPLUGIN: studying membrane complexity in VMD. – Bioinformatics **30**: 1478-1480, 2014.

Gupta S., De Mel J.U., Schneider G.J.: Dynamics of liposomes in the fluid phase. – Curr. Opin. Colloid Interface Sci. **42**: 121-136, 2019.

Higashi Y., Saito K.: Lipidomic studies of membrane glycerolipids in plant leaves under heat stress. – Prog. Lipid Res. **75**: 100990, 2019.

Hollingsworth S.A., Dror R.O.: Molecular dynamics simulation for all. – Neuron **99**: 1129-1143, 2018.

Humphrey W., Dalke A., Schulten K.: VMD: Visual molecular dynamics. – J. Mol. Graph. **14**: 33-38, 1996.

Jo S., Kim T., Im W.: Automated builder and database of protein/membrane complexes for molecular dynamics simulations. – PLoS ONE **2**: e880, 2007.

Jo S., Kim T., Iyer V.G., Im W.: CHARMM-GUI: A web-based graphical user interface for CHARMM. – J. Comput. Chem. **29**: 1859-1865, 2008.

Jo S., Lim J.B., Klauda J.B., Im W.: CHARMM-GUI Membrane Builder for mixed bilayers and its application to yeast membranes. – Biophys. J. **97**: 50-58, 2009.

Jodaitis L., van Oene T., Martens C.: Assessing the role of lipids in the molecular mechanism of membrane proteins. – Int. J. Mol. Sci. **22**: 7267, 2021.

Kirchhoff H., Mukherjee U., Galla H.-J.: Molecular architecture of the thylakoid membrane: lipid diffusion space for plastoquinone. – Biochemistry **41**: 4872-4882, 2002.

Kobayashi K.: Role of membrane glycerolipids in photosynthesis, thylakoid biogenesis and chloroplast development. – J. Plant Res. **129**: 565-580, 2016.

Lee J., Cheng X., Swails J.M. *et al.*: CHARMM-GUI Input Generator for NAMD, GROMACS, AMBER, OpenMM, and CHARMM/OpenMM simulations using the CHARMM36 additive force field. – J. Chem. Theory Comput. **12**: 405-413, 2016.

Lee J., Patel D.S., Ståhle J. *et al.*: CHARMM-GUI Membrane Builder for complex biological membrane simulations with glycolipids and lipoglycans. – J. Chem. Theory Comput. **15**: 775-786, 2019.

Michaud-Agrawal N., Denning E.J., Woolf T.B., Beckstein O.: MDAnalysis: A toolkit for the analysis of molecular dynamics simulations. – J. Comput. Chem. **32**: 2319-2327, 2011.

Parrinello M., Rahman A.: Polymorphic transitions in single crystals: A new molecular dynamics method. – J. Appl. Phys. **52**: 7182-7190, 1981.

Piggot T.J., Allison J.R., Sessions R.B., Essex J.W.: On the calculation of acyl chain order parameters from lipid simulations. – J. Chem. Theory Comput. **13**: 5683-5696, 2017.

Pronk S., Páll S., Schulz R. *et al.*: GROMACS 4.5: a high-throughput and highly parallel open source molecular simulation toolkit. – Bioinformatics **29**: 845-854, 2013.

Rathod A.K., Chavda D., Manna M.: Phase transition and phase separation in realistic thylakoid lipid membrane of marine algae in all-atom simulations. – J. Chem. Inf. Model. **63**: 3328-3339, 2023.

Róg T., Girych M., Bunker A.: Mechanistic understanding from molecular dynamics in pharmaceutical research 2: Lipid membrane in drug design. – Pharmaceuticals **14**: 1062, 2021.

Song Y., Guallar V., Baker N.A.: Molecular dynamics simulations of salicylate effects on the micro- and mesoscopic properties of a dipalmitoylphosphatidylcholine bilayer. – Biochemistry **44**: 13425-13438, 2005.

Thallmair S., Vainikka P.A., Marrink S.J.: Lipid fingerprints and cofactor dynamics of light-harvesting complex II in different membranes. – Biophys. J. **116**: 1446-1455, 2019.

Tieleman D.P., Marrink S.J., Berendsen H.J.: A computer perspective of membranes: molecular dynamics studies of lipid bilayer systems. – BBA-Rev. Biomembr. **1331**: 235-270, 1997.

Tironi I.G., Sperb R., Smith P.E., van Gunsteren W.F.: A generalized reaction field method for molecular dynamics simulations. – J. Chem. Phys. **102**: 5451-5459, 1995.

van Eerden F.J., de Jong D.H., de Vries A.H. *et al.*: Characterization of thylakoid lipid membranes from cyanobacteria and higher plants by molecular dynamics simulations. – BBA-Biomembranes **1848**: 1319-1330, 2015.

van Eerden F.J., Melo M.N., Frederix P.W.J.M. *et al.*: Exchange pathways of plastoquinone and plastoquinol in the photosystem II complex. – Nat. Commun. **8**: 15214, 2017a.

van Eerden F.J., Melo M.N., Frederix P.W.J.M., Marrink S.J.: Prediction of thylakoid lipid binding sites on photosystem II. – Biophys. J. **113**: 2669-2681, 2017b.

van Eerden F.J., van den Berg T., Frederix P.W.J.M. *et al.*: Molecular dynamics of photosystem II embedded in the thylakoid membrane. – J. Phys. Chem. B **121**: 3237-3249, 2017c.

Velitchkova M., Lazarova D., Popova A.: Response of isolated thylakoid membranes with altered fluidity to short term heat stress. – Physiol. Mol. Biol. Plants **15**: 43-52, 2009.

Venable R.M., Krämer A., Pastor R.W.: Molecular dynamics simulations of membrane permeability. – Chem. Rev. **119**: 5954-5997, 2019.

Watkins S.L.: Current trends and changes in use of membrane molecular dynamics simulations within academia and the pharmaceutical industry. – Membranes **13**: 148, 2023.

Wilhelm C., Goss R., Garab G.: The fluid-mosaic membrane theory in the context of photosynthetic membranes: Is the thylakoid membrane more like a mixed crystal or like a fluid? – J. Plant Physiol. **252**: 153246, 2020.

Wu E.L., Cheng X., Jo S. *et al.*: CHARMM-GUI Membrane Builder toward realistic biological membrane simulations. – J. Comput. Chem. **35**: 1997-2004, 2014.

Yesylevskyy S., Rivel T., Ramseyer C.: Curvature increases permeability of the plasma membrane for ions, water and the anti-cancer drugs cisplatin and gemcitabine. – Sci. Rep.-UK **9**: 17214, 2019.

Yesylevskyy S.O., Schäfer L.V., Sengupta D., Marrink S.J.: Polarizable water model for the coarse-grained MARTINI force field. – PLoS Comput. Biol. **6**: e1000810, 2010.